A MODAL ANALYSIS METHOD FOR SLIDER-AIR BEARINGS IN HARD DISK DRIVES

Q. H. Zeng[1] , L. S. Chen[2] and D. B. Bogy

Computer Mechanics Laboratory

Department of Mechanical Engineering

University of California

Berkeley, CA 94720

ABSTRACT

The dynamic characteristics of air-lubricated slider bearings in hard disk drives is an important issue for the drive's performance. A method which can combine numerical and experimental techniques together, and can easily evaluate the system, is not yet available. In this report, we apply the modal analysis technique to analyze the dynamic properties of slider-air bearings, and use modal parameters, such as frequency and damping, to evaluate the system. First, the theoretical background is briefly described. Then, a procedure for the estimation of modal parameters and physical matrices from simulation data is presented. The method is verified, and then used to analyze three slider designs. It is found that the stiffness matrix calculated from neighboring the steady state solutions is much different from the one calculated by the dynamic simulator. The preliminary results indicate that the method may provide a powerful tool for head-medium interface analysis and experiment.

[1] Visiting scholar, Associate professor, Institute of Vibration Engineering, Nanjing University of Aeronuatics & Astronautics, Nanjing, China.

[2] Graduate student

1. INTRODUCTION

Dynamic characteristics of air-lubricated slider bearings is an important issue for lower flying heights, higher relative speeds, faster slider settling times, and more reliable slider-disk interfaces to further improve the performance of hard disk drives. Analyzing the dynamic characteristics requires simultaneously solving the generalized Reynolds equation and the equation of motion of the slider-suspension assembly. Perturbation methods [1,2] have been previously used to obtain approximate solutions. Numerical simulations, such as those provided by the CML Dynamic Simulator[3], have become a powerful and versatile tool for the study of the characteristics and the design of slider-disk interfaces. Because the simulations can solve very complicated configurations, and can obtain the dynamic performance information that is required for the design, they are becoming more widely used in industry.

Experimental techniques have also been applied to study the slider-disk interface to obtain the dynamic characteristics. For example, the effect of surface roughness and disk material on the dynamics of the slider was studied by using measured acoustic emission and vibration signals [4]. However, a method which can combine numerical and experimental techniques together, and can easily evaluate the system, is not yet available. In particular, damping is a very important property of the system, but many papers [4, 5, 6, 7] have only presented qualitative results, and most of the simulation software cannot output the desired damping data. In this report, we apply the modal analysis technique to analyze the dynamic properties of slider-air bearings, and use modal parameters, such as frequency and damping, to evaluate the system. These parameters can be estimated from either numerical simulation results or from measured data. In this report the theoretical background is briefly described. A procedure for the estimation of the modal parameters and physical matrices from simulation data is presented. The method is verified by examples, and used to analyze three slider designs. It is found that the stiffness matrix

calculated from neighboring the steady state solutions is much different from the one calculated by the dynamic simulator, apparently because the squeeze film term in the Reynolds equation significantly affects the modal frequencies and damping ratios of the air bearings. The preliminary results presented here show the method may provide a very useful tool for head-medium interface analysis and experiment.

2. THEORETICAL BACKGROUND

The governing equations for the dynamics of the slider-air bearing-suspension system are the equations of motion of the slider-suspension and the generalized Reynolds equation. Simultaneously solving the equations, the dynamic responses for given disturbances, such as bumps, roughness of the disks, and shock, can be obtained. This can be performed by perturbation methods or numerical simulations. The responses can also be measured by experiments. On the other hand, if we know the disturbances (excitation) and the responses of the system (slider's flying height, pitch, roll, …) to the disturbances, the system can be modeled and characterized. For small disturbances to its steady flying state, the system can be considered as a linear system.

Figure 1 shows a schematic diagram of the slider-air bearing system. Assuming the slider is a rigid body and the system operates in the range near the steady flying state and is linear, time-invariant, conservative, and with viscous damping, the equations of vertical, pitch and roll vibration of the slider can be written as

$$[M]\{\ddot{u}\} + [C]\{\dot{u}\} + [K]\{u\} = \{f(t)\} \tag{1}$$

where $[M]$, $[K]$ and $[C]$ are the mass, stiffness and damping matrices (3x3), and $\{u\}=\{z, p, r\}^T$ is the displacement vector of the slider. In previous methods, the matrices were calculated from the Reynolds and slider's motion equations using small perturbations [2]. In this report, the frequency response functions (FRFs) are calculated from the excitation

and responses. The modal parameters are estimated from the FRFs, and then the matrices can be obtained from these parameters.

2.1 Relationship between the FRFs and the Modal Parameters

Equation (1) is rewritten in state space as

$$[A]\{\dot{y}\}+[B]\{y\}=\{q(t))\} \tag{2}$$

where

$$[A]=\begin{bmatrix} C & M \\ M & 0 \end{bmatrix}_{6\times 6},\quad [B]=\begin{bmatrix} K & 0 \\ 0 & -M \end{bmatrix}_{6\times 6},\quad \{y\}=\begin{Bmatrix} u \\ \dot{u} \end{Bmatrix}_{6\times 1},\quad \{q(t)\}=\begin{Bmatrix} f(t) \\ 0 \end{Bmatrix}_{6\times 1} \tag{3}$$

Assuming $\{q(t)\}=\{0\}$, $\{y\}=\{\phi\}e^{st}$, we can obtain 2N eigenvalues and eigenvectors of the system, s_j, $\{\phi\}_j$, which satisfy the equation

$$\left([A]s_j+[B]\right)\{\phi\}_j=0,\quad j=1,2,\ldots,6 \tag{4}$$

These s_j and $\{\phi\}_j$ will occur in complex conjugate pairs. Constructing an eigenvector matrix as

$$[\Psi]=\begin{bmatrix} \{\phi\}_1 & \{\phi\}_2 & \cdots & \{\phi\}_6 \end{bmatrix} \tag{5}$$

we have the orthogonality properties

$$[\Psi]^T[A][\Psi]=\begin{bmatrix} \ddots & & \\ & a_j & \\ & & \ddots \end{bmatrix} \tag{6}$$

$$[\Psi]^T[B][\Psi]=\begin{bmatrix} \ddots & & \\ & b_j & \\ & & \ddots \end{bmatrix} \tag{7}$$

with

$$s_j=-\frac{b_j}{a_j} \tag{8}$$

or

$$s_j=-2\pi\xi_j f_j+\mathrm{i}2\pi\sqrt{1-\xi_j^2}\,f_j \tag{9}$$

where ξ_j and f_j are the modal damping ratio and the modal frequency of mode j. Performing the Fourier transformation of Eq. (2), gives

$$\left(i\omega[A]+[B]\right)\{Y(\omega)\}=\{Q(\omega)\} \tag{10}$$

or

$$\left[[\Psi]^{-T}\left(i\omega[\Psi]^{T}[A][\Psi]+[\Psi]^{T}[B][\Psi]\right)[\Psi]^{-1}\right]\{Y(\omega)\}=\{Q(\omega)\} \tag{11}$$

Substituting Eqs. (6) and (7) into this equation, we can then solve for *{Y(ω)}* to obtain

$$\{Y(\omega)\}=\sum_{j=1}^{6}\left[\frac{\{\phi\}_j^{T}\{Q(\omega)\}\{\phi\}_j}{a_j(i\omega-s_j)}\right] \tag{12}$$

Therefore, the frequency response function for the response at degree of freedom (DOF) *k*, due to the excitation at DOF *l* will be:

$$H_{kl}(\mathrm{i}\omega)=\sum_{j=1}^{3}\left[\frac{\varphi_{kj}\varphi_{lj}}{a_j(i\omega-s_j)}+\frac{\varphi_{kj}^{*}\varphi_{lj}^{*}}{a_j^{*}\left(i\omega-s_j^{*}\right)}\right],\quad k, l=1,2,3 \tag{13}$$

or

$$H_{kl}(\mathrm{i}\omega)=\sum_{j=1}^{3}\left[\frac{A_{klj}}{(i\omega-s_j)}+\frac{A_{klj}^{*}}{\left(i\omega-s_j^{*}\right)}\right],\quad k, l=1,2,3 \tag{14}$$

where A_{klj} is the residue of mode *j* about DOFs *k* and *l*.

2.2 Modal Parameter Estimation

If we know an approximation to $H_{kl}(\mathrm{i}\omega)$ ($k=1,2,3$) for a given *l* from the numerical simulations or experiments, say as $\overline{H}_{kl}(\mathrm{i}\omega)$, then the modal parameters can be estimated by the following procedure. The first step is curve fitting. Assuming

$$H_{kl}(s)=\frac{N_{kl}(s)}{D(s)} \tag{15}$$

where *D(s)* and $N_{kl}(s)$ are orthogonal polynomials of order *2n* and $2n-1+n_a$ respectively, an error function can be constructed as

$$\varepsilon(s)=\overline{H}_{kl}(s)D(s)-N_{kl}(s) \tag{16}$$

In this equation, *n* is the number of modes, n_a is an additional order to compensate for the noise and out-of-band effects. Let $s=\mathrm{i}2\pi f$, then by use of the least square method, the norm of the errors in the specified frequency band from frequency f_L to f_U is minimized. The coefficients of the polynomials can be estimated. The *2n* roots (poles) s_j ($j=1,2,\ldots 2n$) can be found from *D(s)=0*. The corresponding residues A_{klj} can be calculated by the equation

$$A_{klj} = \left. \frac{N_{kl}(s)}{\mathrm{d}D(s)/\mathrm{d}s} \right|_{s=s_j} \tag{17}$$

The curve fitting can be performed for each FRF separately, or for all FRFs simultaneously. The three modes can be estimated simultaneously (*n=3*), or separately (*n=1* or *2*) through selecting the curve fitting band (f_L and f_U).

After the curve fitting, the six poles and corresponding residues are obtained. They should be in complex conjugate pairs. Then, the second step is mode sorting. Using Eq.(9), the modal frequencies and damping ratios can be calculated. Selecting mode shape scale a_j as

$$a_j = \mathrm{i} \tag{18}$$

where $\mathrm{i} = \sqrt{-1}$, from Eqs. 13 and 14 we will have

$$\begin{Bmatrix} \varphi_{1j}\varphi_{lj} \\ \varphi_{2j}\varphi_{lj} \\ \varphi_{3j}\varphi_{lj} \end{Bmatrix} = \begin{Bmatrix} \mathrm{i}A_{1lj} \\ \mathrm{i}A_{2lj} \\ \mathrm{i}A_{3lj} \end{Bmatrix}, \; j=1,2,3 \tag{19}$$

For given excitation DOF l (*l=1,2* or *3*), the mode shapes can be found from this equation. The estimated mode shapes are often complex. The phase shifts of the shapes will indicate the system has proportional damping if the shifts are very small, or the system has general viscous damping (or non-linear, non-conservative properties) if there are larger shifts.

For the visualization of the mode shapes, the components of the shapes at the eight corners of the slider are calculated in terms of their coordinates using the equation

$$\begin{Bmatrix} \varphi_{xj} \\ \varphi_{yj} \\ \varphi_{zj} \end{Bmatrix}_l = \begin{bmatrix} 0 & 0 & z_l \\ 0 & -z_l & 0 \\ 1 & y_l & x_l \end{bmatrix} \begin{Bmatrix} \varphi_{1j} \\ \varphi_{2j} \\ \varphi_{3j} \end{Bmatrix} \tag{20}$$

where, x_l, y_l ,z_l, are coordinates of corner l with respect to the mass center of the sliders.

2.3 Physical Matrices Estimation

After the modal parameters are obtained, using Eqs.(4) and (5), the physical (mass, stiffness and damping) matrices can be found as

$$\begin{bmatrix} C & M \\ M & 0 \end{bmatrix} = [\Psi]^{-T} \begin{bmatrix} \ddots & & \\ & a_j & \\ & & \ddots \end{bmatrix} [\Psi]^{-1} \tag{21}$$

$$\begin{bmatrix} K & 0 \\ 0 & -M \end{bmatrix} = [\Psi]^{-T} \begin{bmatrix} \ddots & & \\ & b_j & \\ & & \ddots \end{bmatrix} [\Psi]^{-1} \tag{22}$$

For the suspension-slider-air bearing system, the estimated [*M*], [*K*] and [*C*] are effective mass, stiffness and damping matrices of the system.

2.4 Assumptions Verification

Equation (1) implies many assumptions, such as linear, time invariant, conservative, and viscous damping. Before the method is applied, it should be verified in which range the assumptions are satisfied. There are two ways to verify the assumptions. The first is using different excitation levels and/or the different excitation types to excite the system, and checking the changes of the estimated modal parameters. The changes will show some properties of the system. The second way is using the estimated modal parameters to calculate the responses of the slider to the given excitation, and comparing the responses with those obtained from the simulations or experiments without these assumptions. The differences will show whether the assumptions are satisfied, or in which range the results are accurate enough.

2.5 Procedure

The procedure of the modal analysis of the slider-air bearings includes acquiring the FRFs, curve fitting, mode sorting, physical matrices' estimation, verification and application. Acquiring the FRFs is one of the key steps. In this report, we only discuss how to obtain the FRFs from the CML numerical simulator.

First, the steady (or "static") solution should be found by the simulator. Then, a small initial velocity $\dot{z}_0$ of the slider in the vertical direction is specified. The responses of the slider in the three directions are calculated. The responses are subtracted from the steady

solution, and the pure dynamic responses are obtained. These responses are divided by $m\ddot{z}_0$ (m is the slider's mass). The results are the impulse response functions (IRFs) h_{11}, h_{21} and h_{31} of the system. The Fourier transformations of the IRFs are the FRFs H_{11}, H_{21} and H_{31}. Ordinarily, additional FRFs, such as H_{13}, H_{23}, H_{33}, are required because the three modes are not always coupled with the vertical vibration of the center of the slider.

The FRFs have different units, so before the curve fitting is done, it is very important to scale the FRFs to make them have the same units through scale factors. After the mode shapes are obtained, the scale factors are then used to correct the shapes. In the estimation of the physical matrices, scaling is also highly recommended for improving the condition of the $[\psi]$ matrix.

3. CASE STUDIES

3.1 Comparison of three different sliders

Three 50% sliders, “Nutcracker”, Headway AAB and TPC, were used to demonstrate the method. Their air bearing surfaces and pressure profiles are shown in Fig. 2. The dimensions of the sliders are 2.0×1.6×.42 mm. The inertia matrices of the sliders with respect to the sliders' center are

$$\begin{bmatrix} 5.952\times10^{-6} & 0 & 0 \\ 0 & 2.176\times10^{-12} & 0 \\ 0 & 0 & 1.361\times10^{-12} \end{bmatrix} \text{ (kg, m)} \qquad (23)$$

The suspension gimbal is modeled as three springs and dampers. The stiffnesses of the three springs are taken as 18.0 N/m, 1.146×10^{-4} N·m/rad, and 1.432×10^{-4} N·m/rad. The coefficients of the dampers are .002 N·s/m, 1.579×10^{-8} N·m·s/rad, and 1.396×10^{-8} N·m·s/rad. The slider speed relative to the disk is 14.14 m/s (5400 RPM, at the radial position of 25 mm) and without any skew angle. The normal load is 3.5 gram.

The steady flying state pressure profiles on the air bearing surfaces are shown in Figure 2. The steady flying heights at the rail center of the three sliders are about 30.4, 40.6 and 52.4 nm, respectively. The disturbance initial velocities of $\dot{z}_0 = 0.002$ m/s and $\dot{r}_0 = 4$ rad/s were applied separately, and the vertical, pitch and roll responses were calculated. The IRFs and FRFs of the sliders are shown in Figs. 3, 4 and 5. The six FRFs of the each slider are simultaneously fit by using the global orthogonal rational fraction polynomial method. For the "Nutcracker" slider, one curve fitting with three modes is performed. The curve fits (almost coincident with the FRFs) are shown in Fig. 3. However, for the other two sliders, their IRFs in Figs. 4 and 5 show a beat phenomenon because there are two modes with frequencies close to each other. Therefore, two curve fittings with one mode and two modes, respectively, are performed. The curve fits are shown in Figs. 4 and 5. The modal parameters are shown in Tables 1, 2 and 3. As an example, Table 4 shows the mode shapes with respect to the eight corners of the "Nutcracker" slider. Figures 6, 7, and 8 show the mode shapes of the three sliders, respectively. The nodal lines of the modes of the three sliders are shown in Figure 9. The estimated matrices are shown in Tables 5, 6 and 7. All of these results show following points:

❶ The different air bearing surfaces result in substantially different steady flying heights. The "Nutcracker" slider has the smallest flying height, and the TPC slider has largest.

❷ The modal frequencies and shapes of the first mode of the three sliders are very close to each other. The first mode is a coupled pitch and vertical motion. Figures 6, 7 and 8 show the motion of this mode can be approximately represented as a rotation of the slider with respect to the trailing edge. The nodal lines of this mode of the "Nutcracker" and Headway sliders are very near the trailing edge.

❸ The second and third modes of the "Nutcracker" and TPC sliders are very similar; the two sliders have an almost pure roll mode which is a rotational motion about the X axis, and they have close modal frequencies. The nodal lines of the roll mode are almost coincident with the X axis. The two sliders have another coupled pitch and vertical motion which can be considered as a rotation about a line, node line, near the

leading edge. However, the modal frequencies of this mode of the two sliders are very different. This is probably because the "Nutcracker" slider has a sub-ambient pressure and shows a higher stiffness of the air bearing.

❹ The second and third mode shapes of the Headway AAB slider are somewhat different from those of the other two sliders. The nodal lines of the two modes have a shift and rotation, such that the modes are coupled with pitch, roll and vertical motions.

❺ The phase shifts of the three modes of the three sliders are all very small (the shifts of the major components of the shapes, shown in Table 4 as an example, are less than five degrees). That means the three slider-air bearing systems in this range can be approximately considered as systems with proportional damping.

❻ The damping ratios of the “Nutcracker” and Headway AAB sliders are almost the same although their flying heights are different. This is probably because the air bearing surfaces of the two sliders are similar. The TPC slider has relatively higher damping ratios except for the roll mode. The reason might be that the TPC slider dissipates energy by the action of transverse viscous shear on the TPC step surfaces [6].

❼ The estimated mass matrices are very close to the slider's inertia matrix that is shown in Eq.(23) . The slightly larger diagonal elements and non-zero off-diagonal element of the estimated matrices would indicate the errors from the assumptions and/or the calculations. The stiffness matrices will separately be discussed in the later section.

3.2 Verification of the results

To verify these parameters and determine the range of the excitation (or responses) in which the assumptions are approximately satisfied, two calculations were performed for the “Nutcracker” slider. First, a higher excitation level (initial velocities of $\dot{z}_0 = 0.01$ m/s and $\dot{r}_0 = 20$ rad/s) and a lower excitation level (initial velocities of $\dot{z}_0 = 0.0004$ m/s and $\dot{r}_0 = .8$ rad/s) were applied separately, and the modal parameters were estimated and are shown in Table 8. From Table 8, we can see that there are no large differences in the parameters estimated from the three different excitation levels except for the damping

ratio of the third mode. That means the system can be represented as a linear system in this range. Relatively, the third mode is more sensitive to the excitation level because there are larger vibrations at the trailing edge in this mode. For the smallest level, the response of the third mode is very small, such that the calculational errors in the simulation will highly affect the estimation of the damping ratio of this mode.

Second, a sequence of impulse excitations with different levels were applied separately. The initial velocities used in the calculation as the impulse excitations were chosen according to the mode shape as $\{\dot{z}_0, \dot{p}_{0,}\dot{r}_0\}^T = C\{1, 1219, 53.14\}^T$. Only the response of the first mode should be excited. We calculated the pitch response, p_o, using the simulator without the mentioned assumptions, and compared it with the results, p_e, predicted by the estimated modal parameters with the assumptions. Figure 10 shows the comparison of the results for $C=.005$ (maximum vibrational amplitude of the flying height at slider's center is about 13.5 nm). The errors, δ, (about 1.6% for this value of C), are shown in Fig. 11 for the different values of C. They were calculated by

$$\delta = \sum_{n=1}^{Nt} \left[p_e(n\delta t) - p_0(n\Delta t) \right]^2 / \, p_0^2(n\Delta t) \tag{24}$$

The results from the Dynamic Simulator show that the system demonstrates the linear properties in a very wide amplitude range.

3.3 Comparison of the stiffness matrices

We found that the estimated stiffness matrices of the three sliders as presented above are significantly different from the ones directly calculated by using the CML Air Bearing Design Program. As an example, the stiffness matrices of the "Nutcracker" slider are discussed here. Using the Program, the stiffness matrices were calculated as described below in the steady flying state, and are shown in Table 9. These results were obtained by separately giving a small perturbation in the normal load in the vertical, pitch and roll directions, and calculating the steady flying height, pitch and roll with the Program. From

the perturbations and the changes of the height, pitch and roll, we can also obtain an approximate stiffness matrix. For three different perturbation levels, the obtained matrices are shown in Table 9. The table shows the matrices are close to the matrix directly calculated by the Program using the stiffness calculation feature. However, the differences between the matrices are obvious especially for the elements that are related to the vertical and pitch DOFs. There are small differences between the matrices from different perturbation levels. It seems that the system demonstrates small non-linear properties.

The matrix calculated from the modal parameters are much larger than the ones calculated from perturbation of the steady flying state. Because the roll motion is almost decoupled with the vertical and pitch motions, the roll motion of the slider should be the same as the motion of a system with single DOF. The modal frequency f_{roll} of the roll mode can be simply calculated by equation

$$f_{roll} = \frac{1}{2\pi}\sqrt{\frac{K_{33}}{1.361\times10^{-12}}} \tag{25}$$

where K_{33} is the element of the stiffness matrix. The frequencies calculated from the steady and dynamic states will be about 86 kHz and 57 kHz, respectively. Therefore, the results show that the stiffness of the air bearings calculated from the static state (steady flying state calculated by the CML Air Bearing Design Program) is much smaller than the one calculated from the CML Air Bearing Dynamic Simulator. The stiffness of the suspension is much smaller than the one of the air bearings, so the effect of the suspension on the frequencies can be ignored. Therefore, the main difference between the two programs is that the first program does not include the time-dependent squeeze term of the Reynolds equation because the solution is one of the steady state, and the second includes this term. To confirm the effects of this term, the dynamic simulator was modified to eliminate this term, and the modal parameters and stiffness matrix were

calculated through the same procedure as before. The modal frequencies obtained are as follows

1 27.40 kHz
2 59.72 kHz (roll mode)
3 99.29 kHz

The frequency of the roll mode is almost the same as that calculated from the steady state. The stiffness matrix based on this model is shown in Table 9, and it is seen to be much closer to the matrices calculated in the steady state. These results confirm that it is the squeeze term that results in the differences between the two programs, and this term significantly increases the stiffness of the system.

To prevent confusion, we suggest that the stiffness matrix calculated from the steady state method should be called as the "normal load sensitivity matrix", and the stiffness matrix calculated from the dynamic state should be defined as the "stiffness matrix".

4. CONCLUSIONS

A modal analysis method for slider-air bearing systems is proposed. The results of the examples show the assumptions are satisfied in a very wide amplitude range, and the method is convenient and efficient for evaluating the dynamic properties of the systems. Therefore the technique provides a powerful tool for head-medium interface analysis, which can be used with numerical simulations and experiments. It was found that the squeeze term in the Reynolds equation significantly affects the modal frequency. More research work is required to further explain the differences of the stiffness matrices obtained from the "static" state and "dynamic" state. The sensitivity of the modal parameters and experimental methods will also be investigated in the future.

ACKNOWLEDGMENTS

This study is supported by the Computer Mechanics Laboratory at the University of California at Berkeley.

REFERENCES

[1] K. Ono, "Dynamic Characteristics of Air-Lubricated Slider Bearing for Noncontact Magnetic Recording", J. of Lubrication Technology, Apr. 1975, pp.250-260.

[2] P. W. Smith and W.D. Iwan, "Dynamic Figures of Merit for the Design of Gas-Lubricated Slider Bearings", ASME, Adv. in Info. Storage Syst. V.3, 1991, pp.41-53.

[3] Y. Hu and D. B. Bogy, "The CML Air Bearing Dynamic Simulator", Technical Report No. 95-011, Computer Mechanics Lab., Dept. of Mechanical Engineering, University of California at Berkeley, 1995.

[4] S. Suzuki and H. Nishihira, "Study of Slider Dynamics over Very smooth Magnetic Disks", J. of Tribology (95-Trib-38).

[5] Y. Hu, "Head-Disk-Suspension Dynamics", Ph.D Dissertation, Dept. of Mechanical Engineering, University of California at Berkeley, Apr. 1996.

[6] J. W. White, "Flying Characteristics of the Transverse and Negative Pressure Contour ('TNP") Slider Air Bearing", (96-Trib-8).

[7] J. W. White, "The Transverse Pressure Contour Slider: Flying Characteristics and Comparison with Taper-Flat and Cross-Cut Type Sliders", ASME, Adv. in Info. Storage Syst., Vol. 3, pp. 1-14.

No	Freq.	Damping ratio	Mode Shape and its scale						
			a_j	φ_{1j}		φ_{2j}		φ_{3j}	
j	(kHz)	(%)		Amp.	Phase	Amp.	Phase	Amp.	Phase
1	56.49	4.65	i	.3912	-1.5	480.8	-2.0	20.83	1.5
2	84.31	4.57	i	.0072	-175.9	7.378	174.4	818.5	-0.5
3	123.46	4.49	i	.1860	-175.7	425.6	4.8	1.845	-177.8

Table 1 Estimated modal parameters of the "**Nutcracker**" slider ($i = \sqrt{-1}$ in the table)

No	Freq.	Damping Ratio	Modal shape and its scale						
			a_j	φ_{1j}		φ_{2j}		φ_{3j}	
j	(kHz)	(%)		Amp.	Phase	Amp.	Phase	Amp.	Phase
1	48.48	4.65	i	.4026	-1.5	570.4	-1.7	.7061	83.8
2	97.93	3.96	i	.2008	1.5	373.2	180.0	385.8	-9.0
3	101.06	4.28	i	.1220	170.5	235.7	-8.7	642.6	3.8

Table 2 Estimated modal parameters of the **Headway AAB** slider

No	Freq.	Damping Ratio	Modal shape and its scale						
			a_j	φ_{1j}		φ_{2j}		φ_{3j}	
j	(kHz)	(%)		Amp.	Phase	Amp.	Phase	Amp.	Phase
1	45.17	6.71	i	.3758	-3.3	663.0	-3.5	3.845	141.1
2	73.08	4.48	i	.2992	3.8	437.6	177.5	125.1	-33.6
3	74.57	5.58	i	.0434	149.3	69.76	-23.6	884.7	0.0

Table 3 Estimated modal parameters of the **TPC** slider

Mode	Node	X (Amp	Phase)	Y (Amp	Phase)	**Z (Amp**	**Phase)**
1	1	**1.003E-01**	**177.9**	4.368E-03	1.2	**8.527E-01**	**-2.0**
	2	**1.003E-01**	**177.9**	4.368E-03	1.2	**1.021E-01**	**177.1**
	3	**1.003E-01**	**177.9**	4.368E-03	1.2	**8.859E-01**	**-1.9**
	4	**1.003E-01**	**177.9**	4.368E-03	1.2	**6.894E-02**	**175.2**
	5	**1.003E-01**	**-2.1**	4.368E-03	-178.8	**8.527E-01**	**-2.0**
	6	**1.003E-01**	**-2.1**	4.368E-03	-178.8	**1.021E-01**	**177.1**
	7	**1.003E-01**	**-2.1**	4.368E-03	-178.8	**8.859E-01**	**-1.9**
	8	**1.003E-01**	**-2.1**	4.368E-03	-178.8	**6.894E-02**	**175.2**
2	1	1.771E-03	-18.2	**1.719E-01**	**-0.7**	**6.696E-01**	**179.2**
	2	1.771E-03	-18.2	**1.719E-01**	**-0.7**	**6.536E-01**	**179.6**
	3	1.771E-03	-18.2	**1.719E-01**	**-0.7**	**6.398E-01**	**-0.6**
	4	1.771E-03	-18.2	**1.719E-01**	**-0.7**	**6.559E-01**	**-1.1**
	5	1.771E-03	161.8	**1.719E-01**	**179.3**	**6.696E-01**	**179.2**
	6	1.771E-03	161.8	**1.719E-01**	**179.3**	**6.536E-01**	**179.6**
	7	1.771E-03	161.8	**1.719E-01**	**179.3**	**6.398E-01**	**-0.6**
	8	1.771E-03	161.8	**1.719E-01**	**179.3**	**6.559E-01**	**-1.1**
3	1	**9.050E-02**	**-177.9**	4.069E-04	-174.6	**2.442E-01**	**2.5**
	2	**9.050E-02**	**-177.9**	4.069E-04	-174.6	**6.178E-01**	**-178.0**
	3	**9.050E-02**	**-177.9**	4.069E-04	-174.6	**2.411E-01**	**2.5**
	4	**9.050E-02**	**-177.9**	4.069E-04	-174.6	**6.209E-01**	**-178.0**
	5	**9.050E-02**	**2.1**	4.069E-04	5.4	**2.442E-01**	**2.5**
	6	**9.050E-02**	**2.1**	4.069E-04	5.4	**6.178E-01**	**-178.0**
	7	**9.050E-02**	**2.1**	4.069E-04	5.4	**2.411E-01**	**2.5**
	8	**9.050E-02**	**2.1**	4.069E-04	5.4	**6.209E-01**	**-178.0**

Table 4 Estimated modal shapes of the "**Nutcracker**" slider with respective to the eight corners of the sliders

Matrix	Estimated
Mass	6.135D-06 -1.439D-10 -4.026D-14 -1.439D-10 2.244D-12 1.115D-15 -4.026D-14 1.115D-15 1.408D-12
Stiffness	1.832D+06 -8.769D+02 -6.507D+00 -8.769D+02 9.835D-01 -4.035D-03 -6.507D+00 -4.035D-03 3.958D-01
Damp.	4.765D-01 -3.358D-04 -2.315D-06 -3.358D-04 3.033D-07 5.169D-10 -2.315D-06 5.169D-10 5.419D-08

Table 5 Estimated physical matrices of the "**Nutcracker**" slider

Matrix	Estimated
Mass	6.010D-06 -1.729D-10 4.081D-11 -1.729D-10 2.279D-12 -5.223D-14 4.081D-11 -5.223D-14 1.444D-12
Stiffness	1.359D+06 -5.796D+02 8.630D-01 -5.796D+02 6.104D-01 -2.887D-03 8.630D-01 -2.887D-03 5.711D-01
Damp.	7.894D-02 1.182D-05 -1.745D-05 1.182D-05 1.995D-09 2.457D-08 -1.745D-05 2.457D-08 9.485D-08

Table 6 Estimated physical matrices of the "**Headway AAB**" slider

Matrix	Estimated
Mass	6.183D-06 -3.095D-10 2.401D-11 -3.095D-10 2.320D-12 -3.360D-14 2.401D-11 -3.360D-14 1.354D-12
Stiffness	9.697D+05 -2.877D+02 4.897D+00 -2.877D+02 3.384D-01 -3.607D-03 4.897D+00 -3.607D-03 2.975D-01
Damp.	3.281D-01 -8.065D-05 5.677D-06 -8.065D-05 3.989D-09 1.104D-08 5.677D-06 1.104D-08 6.034D-08

Table 7 Estimated physical matrices of the "**TPC**" slider

	Mode No	Excitation Level (.0004, .8, .8)	Excitation Level (.002, 4, 4)	Excitation Level (.01, 20, 20)
Modal	1	56.49	56.49	56.34
Frequency	2	84.31	84.31	84.52
(kHz)	3	123.7	123.5	123.1
Damping	1	4.87	4.65	4.68
Ratio	2	4.57	4.57	4.69
(%)	3	2.36	4.49	4.44

Table 8 Modal frequencies and damping ratios of the "**Nutcracker**" slider estimated from different excitation levels

State of air bearing	Method and Parameters	"Stiffness matrix"
Steady	Directly calculated by the CML Air Bearing Design Program (Give perturbation in the steady flying attitude, calculate the attitude change)	7.361e+05 6.335e+02 1.126e+01 4.106e+02 5.261e-01 -1.536e-02 -1.192e+01 1.311e-02 1.751e-01
	Separately give **-0.1 (g or g-mm)** perturbation in the suspension load, calculate steady flying attitude change.	8.124e+05 7.655e+02 -1.375e+01 5.413e+02 6.936e-01 -3.772e-03 1.595e+02 2.091e-01 1.789e-01
	Separately give **0.1 (g or g-mm)** perturbation in the suspension load, calculate steady flying attitude change.	9.459e+05 8.651e+02 5.905e+01 5.220e+02 6.457e-01 4.760e-02 -4.224e+01 -3.584e-02 1.690e-01
	Separately give **0.2 (g or g-mm)** perturbation in the suspension load, calculate steady flying attitude change.	8.983e+05 8.282e+02 7.003e+01 4.717e+02 5.912e-01 5.490e-02 2.126e+01 2.335e-02 1.796e-01
Dynamic	Separately give initial velocities, calculate dynamic responses **with squeeze term**, then identify modal parameters, calculate the matrix from the parameters	1.832D+06 -8.769D+02 -6.507D+00 -8.769D+02 9.835D-01 -4.035D-03 -6.507D+00 -4.035D-03 3.958D-01
	Separately give initial velocities, calculate dynamic responses **without squeeze term**, then identify modal parameters, calculate the matrix from the parameters	6.311D+05 -5.804D+02 -1.073D+00 -5.804D+02 7.164D-01 2.512D-03 -1.073D+00 2.512D-03 2.020D-01

Table 9 Stiffness matrices of the "nutcracker" slider

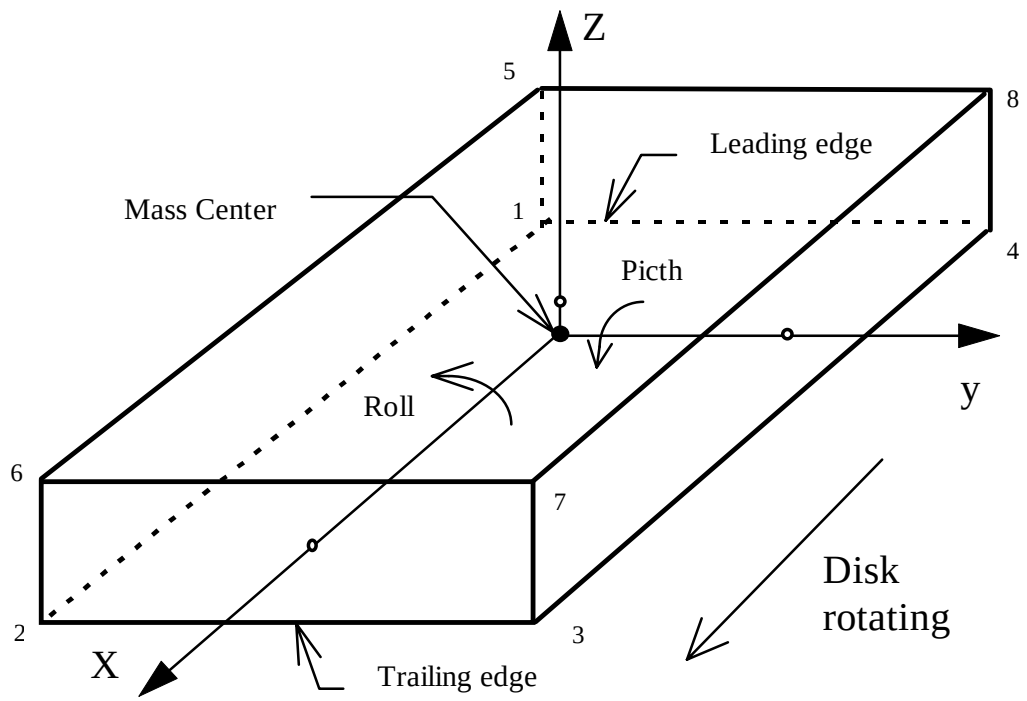

Figure 1 Schematic diagram of the slider-air bearing system

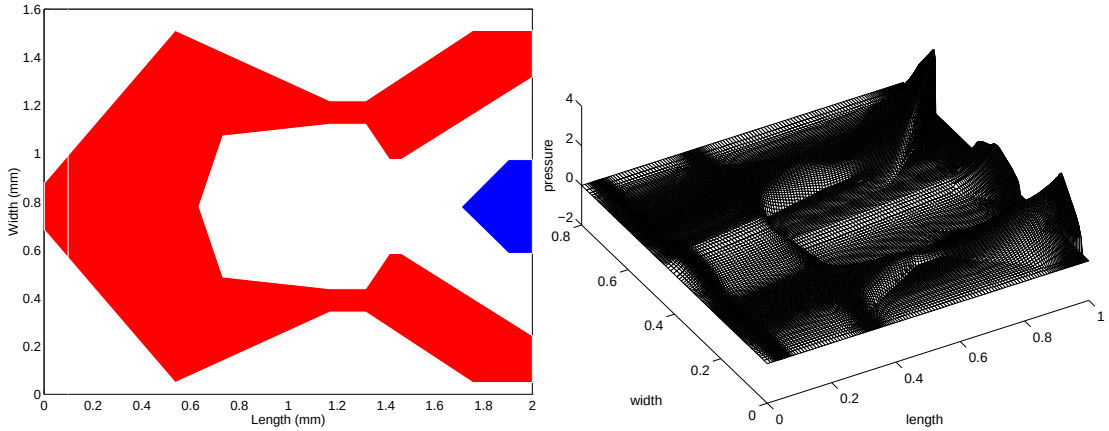

(a) The "Nutcracker" slider

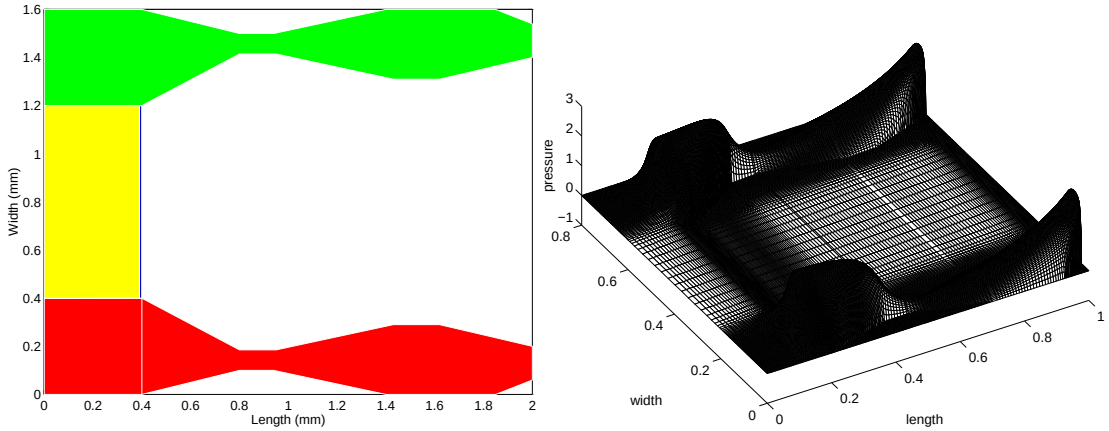

(b) The headway AAB slider

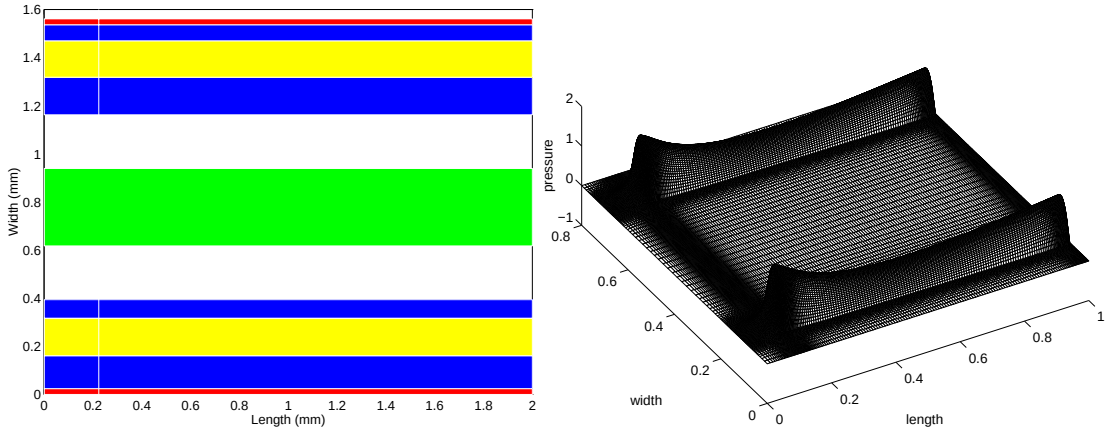

(c) The TPC slider

Figure 2 Air bearing surfaces and pressure profiles of the sliders

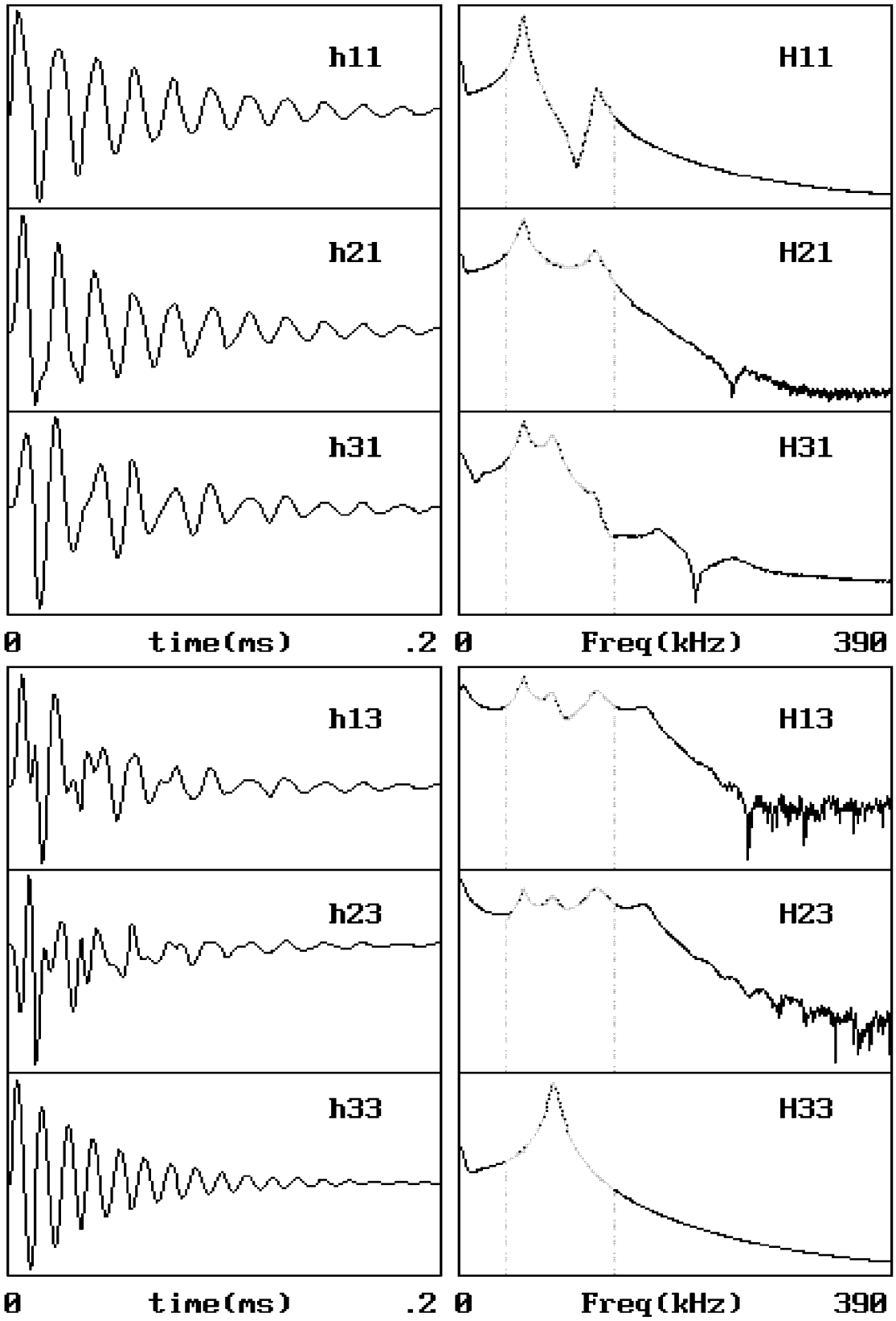

Figure 3 IRFs (left), FRFs (right, solid), and curve fits (right, dot, almost coincident with the FRFs) of the "**Nutcracker**" slider

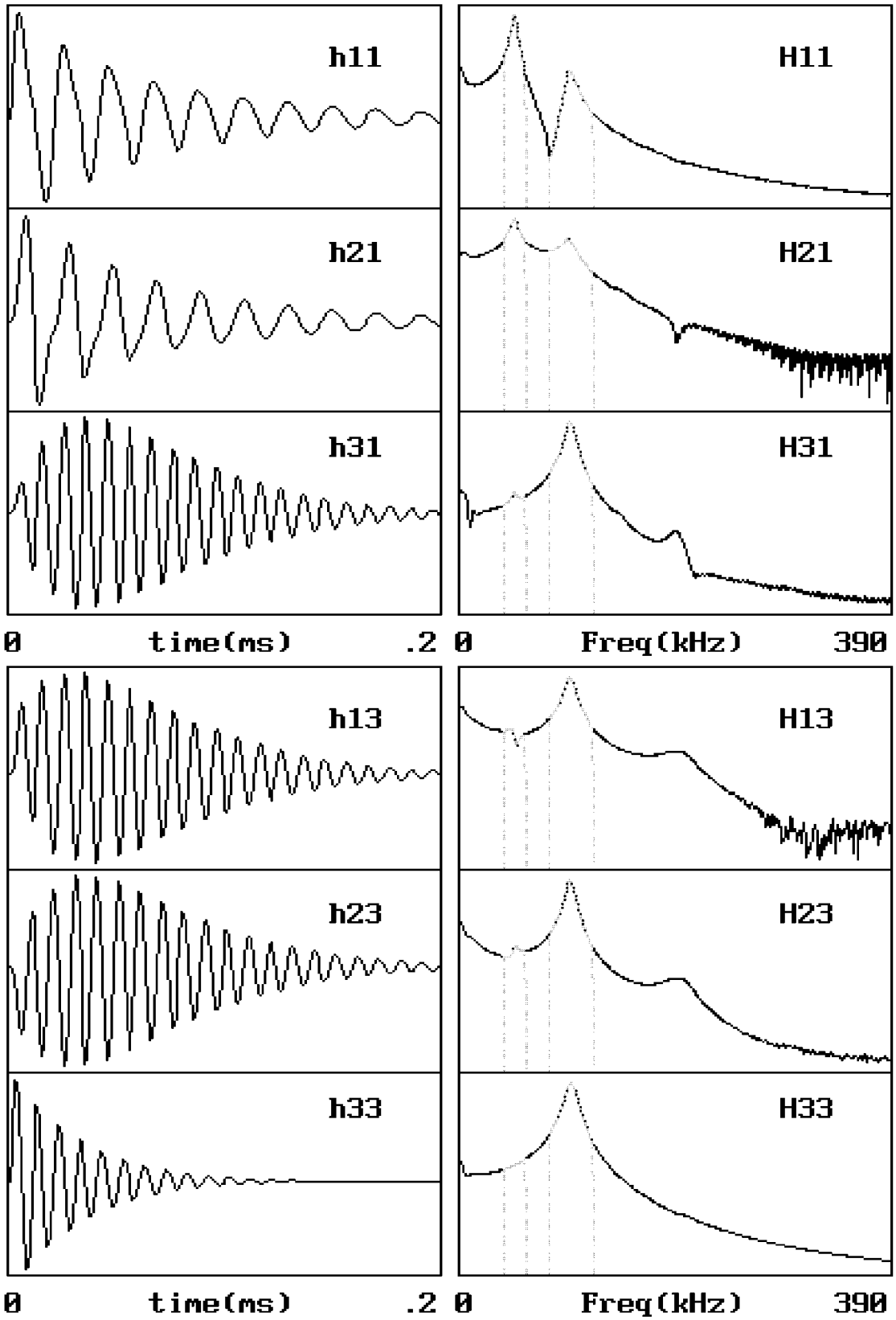

Figure 4 IRFs (left), FRFs (right, solid), and curve fits (right, dot, almost coincident with the FRFs) of the **Headway AAB** slider

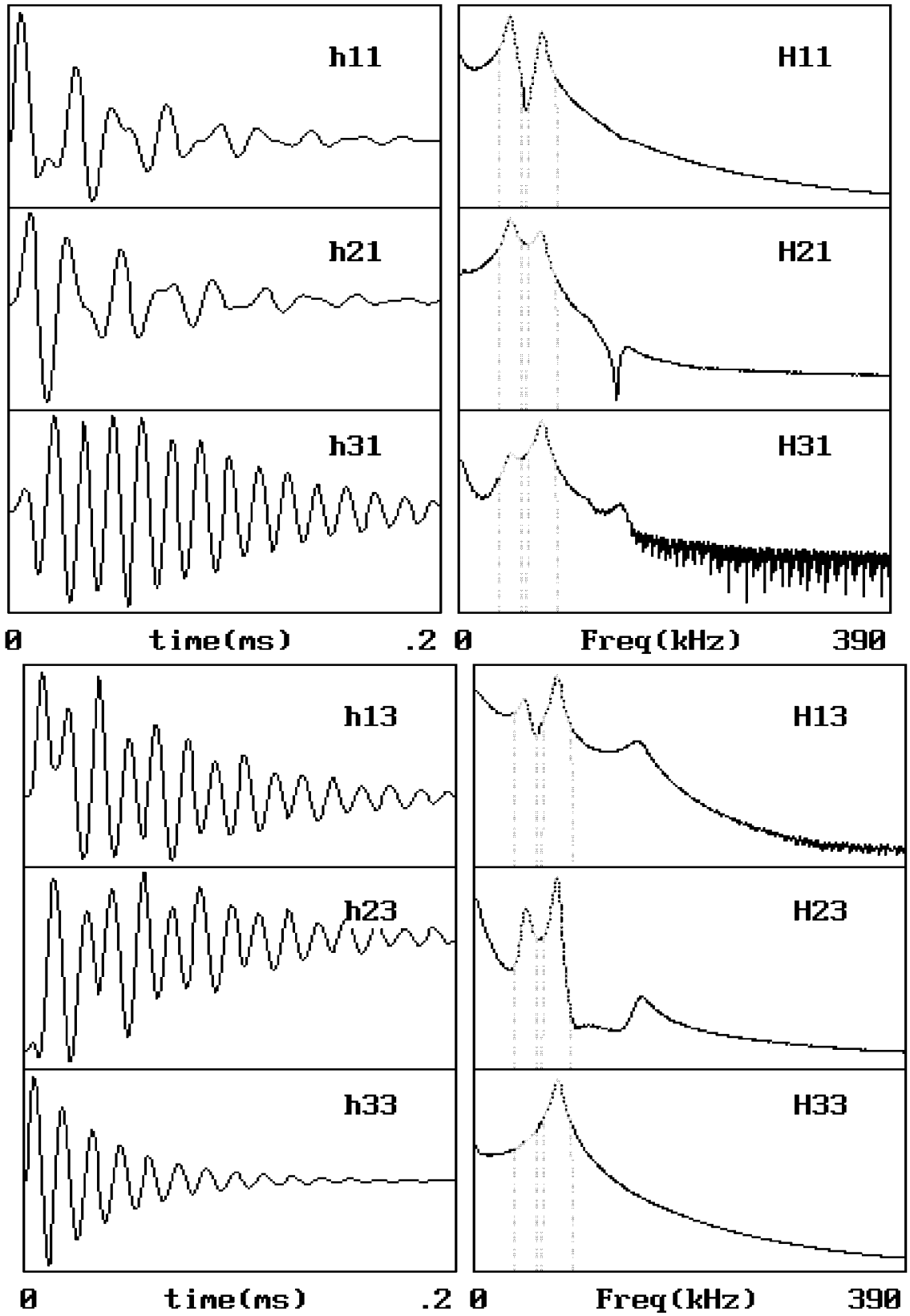

Figure 5 IRFs (left), FRFs (right, solid), and curve fits (right, dot, almost coincident with the FRFs) of the **TPC** slider

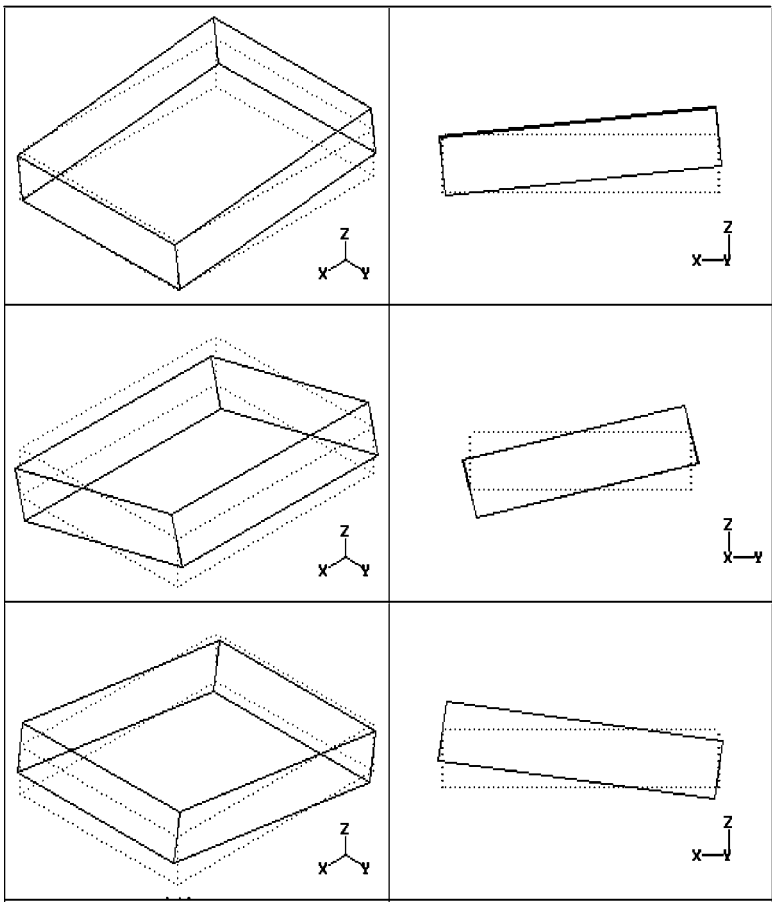

Mode: 1
Frequency: 56.49 kHz
Damping Ratio: 4.65 %

Mode: 2
Frequency: 84.31 kHz
Damping Ratio: 4.57 %

Mode: 3
Frequency: 123.5 kHz
Damping Ratio: 4.49 %

Figure 6 Mode shapes of the "**Nutcracker**" slider

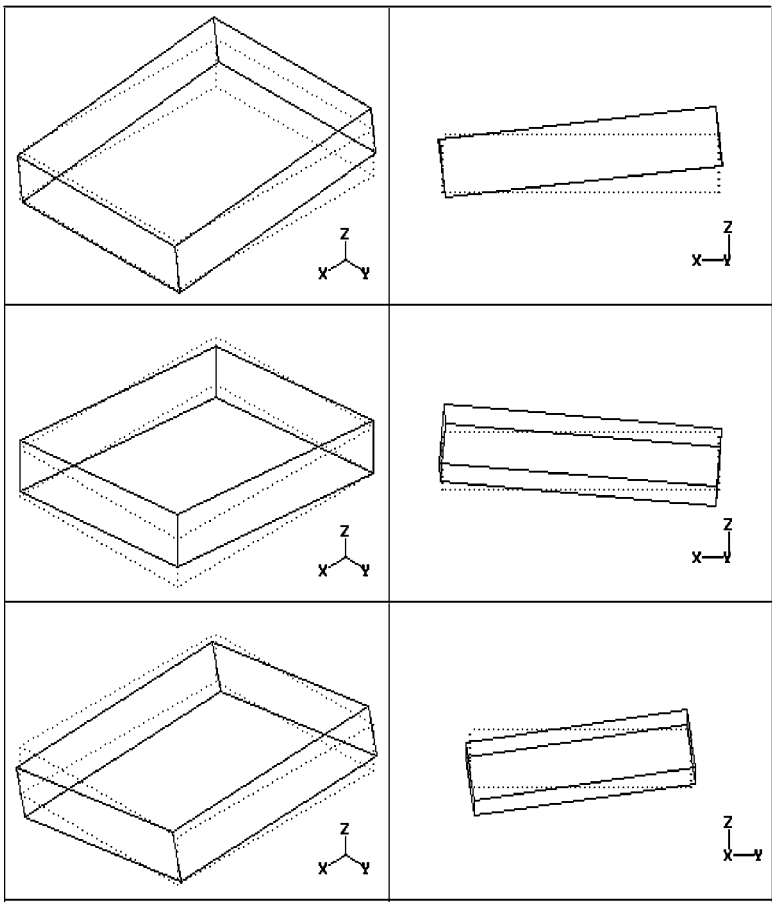

Mode: 1
Frequency: 48.48 kHz
Damping Ratio: 4.65 %

Mode: 2
Frequency: 97.93 kHz
Damping Ratio: 3.96 %

Mode: 3
Frequency: 101.1 kHz
Damping Ratio: 4.28 %

Figure 7 Mode shapes of the **Headway AAB** slider

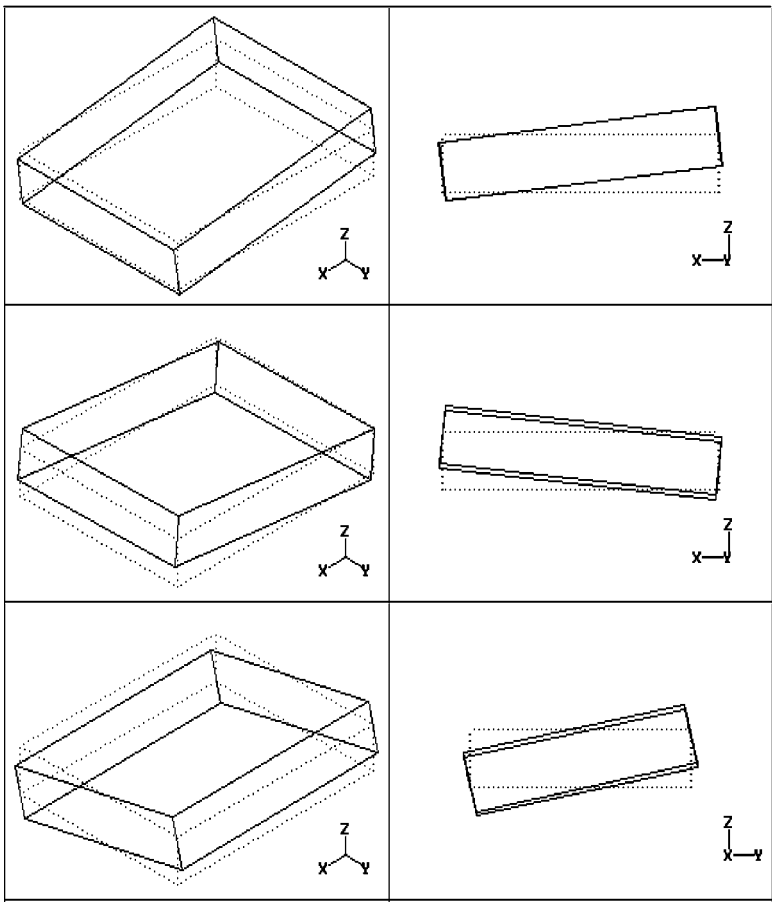

Mode: 1
Frequency: 45.17 kHz
Damping Ratio: 6.71 %

Mode: 2
Frequency: 73.08 kHz
Damping Ratio: 4.48 %

Mode: 3
Frequency: 74.57 kHz
Damping Ratio: 5.58 %

Figure 8 Mode shapes of the **TPC** slider

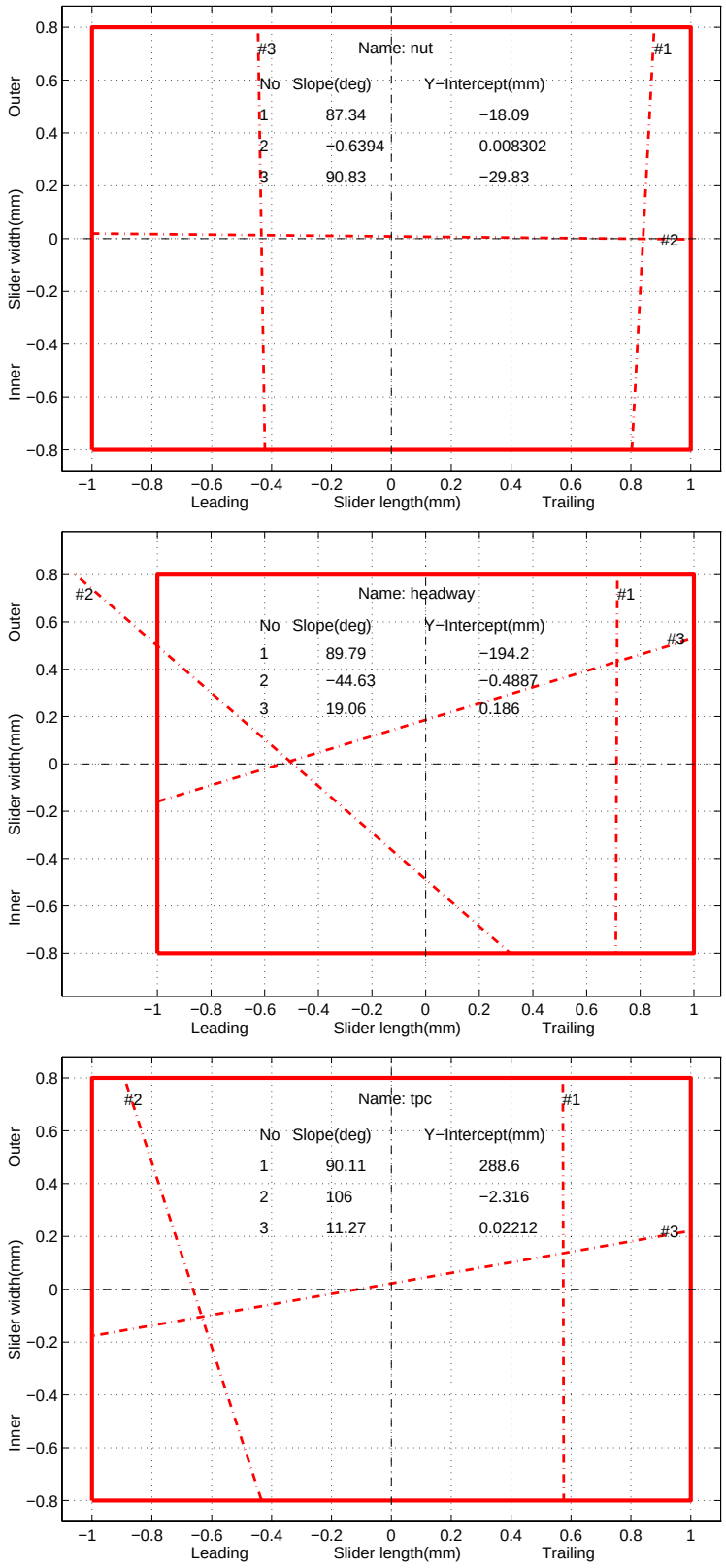

Figure 9 Nodal lines of the modes of the three sliders

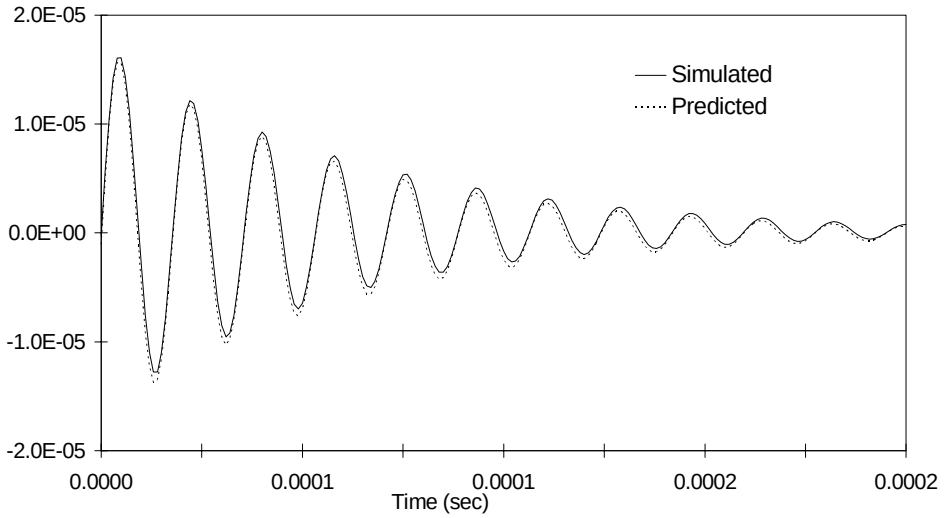

Figure 10 Comparison of the pitch responses (C=.005)

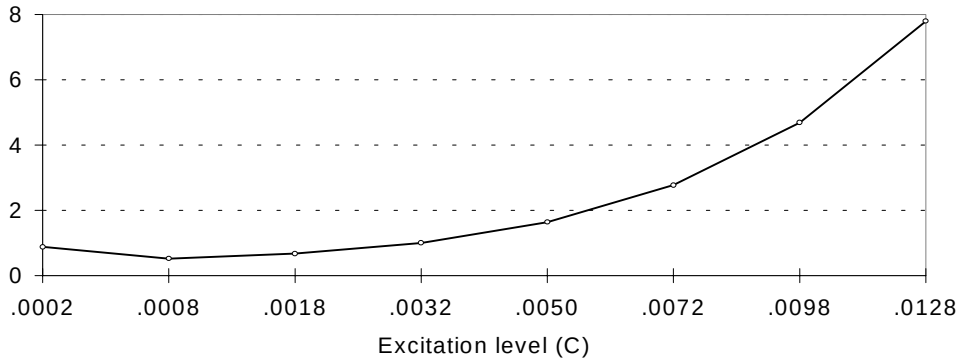

Figure 11 The errors (%) of the predicted responses for different excitation levels